CrystEngComm

PAPER

View Article Online
View Journal | View Issue

Cite this: *CrystEngComm*, 2014, **16**, 6213

Water channels and zipper structures in Schiff base-like Cu(II) and Ni(II) mononuclear complexes†

Charles Lochenie,[ab] Stephan Schlamp,[a] Antoine P. Railliet,[b] Koen Robeyns,[b] Birgit Weber[a] and Yann Garcia*[b]

Received 4th April 2014,
Accepted 9th May 2014

DOI: 10.1039/c4ce00710g

www.rsc.org/crystengcomm

The crystal structures of four Cu(II) complexes and one Ni(II) complex bearing a square planar N_2O_2 coordination sphere are discussed. In all cases a distorted square planar coordination sphere is observed that is independent of the metal centre and the ligand and is only influenced by the packing of the molecules in the crystal. For the less distorted copper complexes metal–aromatic interactions are observed, while no significant intermolecular interactions are found for the nickel complexes. This can be explained by the different electronic character of Cu(II) and Ni(II) and is also reflected in the differences in the solvatochromism of these complexes.

Introduction

Numerous complexes of Schiff base ligands are investigated due to their high potential as catalysts,[1,4,5] biological agents,[2,6] model compounds for active centres of metalloenzymes[3] (*e.g.* galactose oxidase[7] for Cu(II)), magnetic materials,[3] *etc.* Many of the crystal structures of Cu(II) complexes show either a (distorted) square planar or a square pyramidal coordination sphere.[5,6,8–10] In some cases interesting crystal packings such as "zipper" structures are observed.[10] Another interesting facet is the solvatochromism of such copper complexes that can be observed in both solution and the solid state.[9,11] Here we report X-ray crystal structures of a $N_2O_2^{2-}$-coordinating Schiff base-like ligand and its Cu(II) and Ni(II) complexes, the synthesis of which was first described in 1966.[12] The influence of the crystallisation solvent on the crystal packing of the copper complexes explains why solvatochromism was observed in solution but not for the analogous nickel complexes.[12]

Results and discussion

Synthesis of the complexes

The synthesis pathway as well as the structures of both ligands and complexes are shown in Scheme 1. Complexes can be obtained by mixing H_2Lx with a metal acetate in methanol. After stirring at room temperature, complexes precipitate to **1** and **2**.[12] Refluxing the reaction mixture was proven unnecessary by comparison of the IR spectra of the refluxed and stirred compounds. The [CuL1] (**1**) and [CuL2] (**3**) complexes were both obtained as a brown powder and the [NiL1] (**2**) complex as an orange powder. The solutions of the nickel complex have the same orange colour, whereas for the copper complex different shades of brown were observed, from very dark brown (in $CDCl_3$) to brown (in methanol, ethanol, water or THF). The pyridine solutions are all green.[12]

Crystal structures

H_2L1·0.5dioxane. The synthesis of the ligand has been described,[12] but its crystal structure has not. The molecule crystallises in the space group *C*2/*c* and the asymmetric unit contains one molecule of the ligand for half a molecule of dioxane. An ORTEP drawing is given in Fig. 1. Of special interest is the equilibrium between the keto–enamine tautomer and the imino–enol tautomer of the molecule, which is typical of these Schiff base-like ligands (Scheme 2).

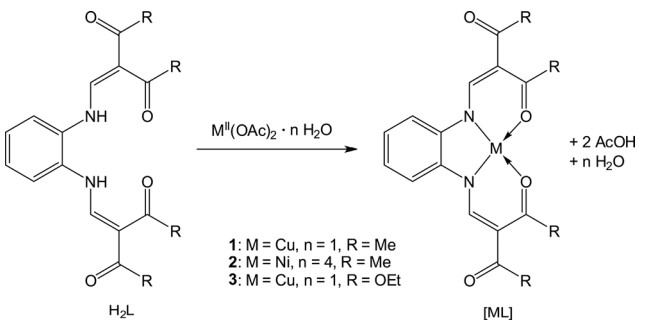

Scheme 1 Synthesis pathway for the synthesis of **1**, **2** and **3**.

[a] *Inorganic Chemistry II, Universität Bayreuth, Universitätsstraße 30, NW 1, 95440 Bayreuth, Germany*
[b] *Institute of Condensed Matter and Nanosciences, Molecules, Solids and Reactivity (IMCN/MOST), Université Catholique de Louvain, Place L. Pasteur 1, 1348 Louvain-la-Neuve, Belgium. E-mail: yann.garcia@uclouvain.be; Fax: +32 10472330; Tel: +32 10472826*

† Electronic supplementary information (ESI) available: Fig. S1 and S2. CCDC 995462–995467 for H_2L1·0.5dioxane, **1**·$CHCl_3$, **1**·$2H_2O$, **1**·*x*solv, **2**·MeOH and **3**. For ESI and crystallographic data in CIF or other electronic format see DOI: 10.1039/c4ce00710g

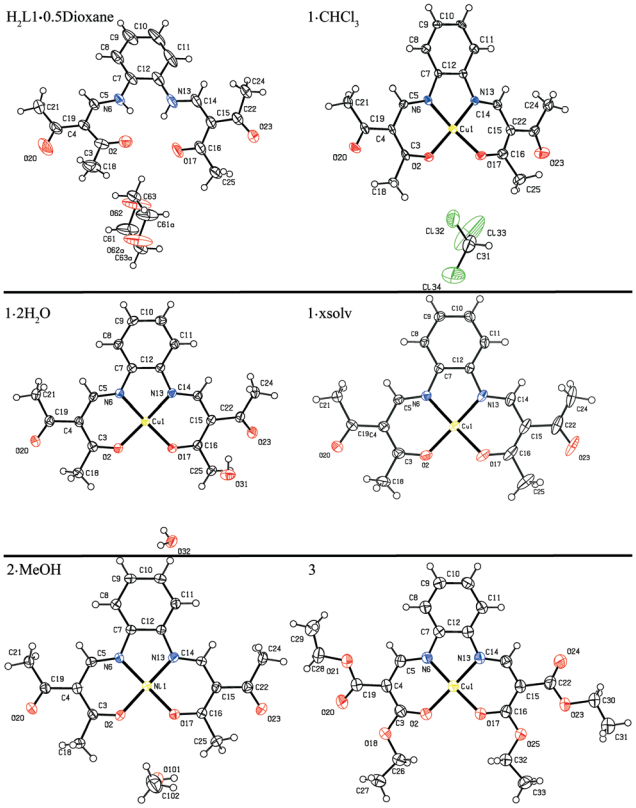

Fig. 1 An ORTEP[14] drawing of the asymmetric unit with thermal ellipsoids shown at the 50% probability level.

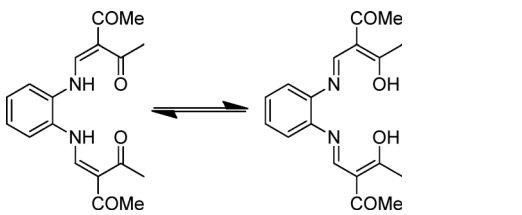

Scheme 2 Equilibrium between the keto–enamine tautomer (left) and the imino–enol tautomer (right).

An equilibrium between these two forms can lead to thermo- and photochromism.[15] The reported C=O bond lengths (between 1.21 and 1.25 Å) indicate that the keto–enamine form is favoured (a CSD search on similar substructures yielded an average value of 1.219 Å for C=O and 1.423 Å for C–OH). This is in agreement with the X-ray structures of a similar ligand,[16] and in contrast to other Schiff base ligands like salen (*N*,*N*′-ethylenebis(salicylimine)), where the imino–enol form is preferred. The ligand is not planar and the angles between the planes, calculated through the 'arms' of the ligand, is 39.89°. Two intra-molecular hydrogen bonds are located between the enamine and ketone functions. Hydrogen bond distances and angles for all reported crystal structures are reported in Table 1. The crystal packing is shown in the ESI, Fig. S1.†

Copper and nickel complexes. Copper complex **1** crystallizes as three solvates. From trichloromethane, **1**·$CHCl_3$ crystallizes in the space group *Aba*2. Using tetrahydrofuran as solvent yields **1**·$2H_2O$ which crystallizes in the space group *Pbca* while a MeOH–EtOH mixture affords **1**·*x*solv with an undefined number of disordered non-coordinating solvent molecules (most likely water and methanol) which crystallizes in the space group $P2_1/c$.

Single crystals of **3**, although prepared in methanol, did not include any solvent molecules unlike the nickel complex **2**·MeOH. The asymmetric unit of the five structures is shown in Fig. 1. Selected bond lengths and angles are reported in Table 2. Both the copper and nickel centres sit in a square planar N_2O_2 coordination sphere. The average coordination bond lengths are 1.91 Å (Cu–O and Cu–N), whereas for **2**·MeOH, the bond lengths are shorter with 1.84 Å (Ni–N) and 1.85 Å (Ni–O), which can be solely attributed to the smaller

Table 1 Short intermolecular contacts (distances (Å) and angles (°)) of H_2L1·0.5dioxane, **1**·$CHCl_3$, **1**·$2H_2O$ and **2**·MeOH

D–H···A	D–H	H···A	D···A	D–H···A	Type
H_2L1·0.5dioxane					
N6–H6···O2	0.88	1.87	2.561(4)	134	Intra
N6–H6···O2	0.88	2.35	2.740(4)	107	Intra
N13–H13···O17	0.88	1.90	2.558(4)	130	Intra
(1·$2H_2O$)					
O31–H31A···O2[a]	0.82	2.53	3.224(3)	144	
O31–H31A···O17[a]	0.82	2.41	3.146(3)	150	
O31–H31B···O32[b]	0.82	1.97	2.789(3)	178	
O32–H32A···O23[c]	0.82	2.11	2.932(3)	176	
O32–H32B···O31[d]	0.82	1.98	2.792(3)	176	
(2·MeOH)					
O101–H101···O23[e]	0.84	1.99	2.826(6)	179	

[a] 1 + x, y, z. [b] 1/2 + x, 1/2 − y, 1 − z. [c] 1/2 − x, 1/2 + y, z. [d] − 1 + x, y, z. [e] 1 − x, −y, 1 − z.

Table 2 Selected bond lengths (Å) and angles (°) of complexes **1**·$CHCl_3$, **1**·$2H_2O$, **1**·*x*solv, **2**·MeOH and **3** (M=Cu, Ni)

Bonds	1·$CHCl_3$	1·$2H_2O$	1·*x*solv
M–O2	1.905(3)	1.9081(18)	1.909(2)
M–O17	1.897(3)	1.9153(18)	1.911(2)
M–N6	1.906(3)	1.915(2)	1.914(2)
M–N13	1.910(4)	1.911(2)	1.907(2)
	2·MeOH	3	
M–O2	1.848(3)	1.9191(15)	
M–O17	1.852(3)	1.9143(16)	
M–N6	1.836(3)	1.9051(18)	
M–N13	1.843(3)	1.9114(18)	
Angles	1·$CHCl_3$	1·$2H_2O$	1·*x*solv
O2–M–O17	89.39(13)	89.44(7)	89.10(9)
O2–M–N6	92.99(14)	92.47(8)	92.55(9)
O17–M–N13	92.52(14)	92.64(8)	92.49(10)
N6–M–N13	86.05(15)	85.45(8)	85.98(9)
O2–M–N13	173.74(16)	177.92(8)	174.52(10)
O17–M–N6	170.93(18)	177.64(8)	177.93(10)
	2·MeOH	3	
O2–M–O17	85.98(13)	89.32(7)	
O2–M–N6	93.68(14)	93.16(7)	
O17–M–N13	93.45(14)	92.27(7)	
N6–M–N13	87.04(15)	85.40(8)	
O2–M–N13	177.67(14)	176.40(7)	
O17–M–N6	176.31(14)	176.32(8)	

covalent radius of Ni (124 pm) with respect to Cu (132 pm). In the case of **1**·$CHCl_3$ the square planar coordination sphere is slightly distorted with both coordinating oxygen atoms slightly above and below the N–Cu–N plane. The distortion can be appraised through the sum of the angles in the coordination sphere. In a perfect square planar geometry the sum of the angles is $\sum$ = 720° whereas for a tetrahedral coordination geometry $\sum$ = 656.82°. In the case of **1**·$CHCl_3$, $\sum$ = 705.6° indicating some distortion, however, it is close to the theoretical value for a square planar geometry. For the other complexes, an increase is noticed with $\sum$ = 712.6° and 712.9° for **1**·*x*solv and **3**, respectively; $\sum$ = 714.1° for **2**·MeOH and $\sum$ = 715.6° for **1**·$2H_2O$, indicating a decrease in the distortion of the square planar geometry. Another way to evaluate the distortion is to measure the angle between the N–M–N and the O–M–O planes. For **1**·$CHCl_3$ this angle is 11.0° and it decreases in the order **1**·*x*solv (5.5°), **2**·MeOH and **3** (both 4.4°) to **1**·$2H_2O$ (1.4°) displaying the same sequence as that obtained for the sum of the angles.

Crystal packing considerations. The similarities in the molecular structures are also conserved in the crystal packing. All metal complexes of **1** show conserved stacking arrangements, with parallel alignment of the planar complexes and similar twist angles between neighbouring molecules (see Fig. 2). Even the non-planar free ligand shows comparable twist angle and intermolecular distance (Fig. S11, ESI†).

Despite the variety in the space groups and unit cell parameters observed for **1** and **2**, all show a similar packing behaviour. The stacks of parallel oriented molecules are inclined with respect to the stacking direction and looking at the stacks one observes a similar orientation of the molecules. When water or methanol was used to crystallize the complexes, the solvent molecules are confined to one-directional channels alongside the columns of **1**. In the case of $CHCl_3$ these channels are too small to accommodate the solvent atoms and the columns of **1** are pushed away leaving a layer of $CHCl_3$, resulting in the elongation of the unit cell parameters (~27 Å for **1**·$CHCl_3$ as opposed to ~23 Å for the remaining complexes of **1** and **2**). This might suggest that π–π or metal–π interactions are responsible for the order within the stacks and that the choice of the solvent influences the position of the columns relative to one another, where the water or methanol channels stabilize the packing through hydrogen bonds (see Table 1). The intermolecular distance in the 3rd direction is controlled by the inclination of the complexes with respect to the stacks (Table 3). Water channels within the packing of **1** propagate as a 4_1 screw chain along the [100] axis. One of the hydrogen atom bonds to the stacked complexes while the other one bonds to the next water molecule. Fig. 3 shows the unit cell packing of **1**·$CHCl_3$ and **1**·$2H_2O$; the packing diagrams of the other complexes can be found in the ESI (S1–S10†).

While the copper complex **3** also stacks in (loose) piles, the other complexes are rotated 180° with respect to one another.

The molecule is slightly distorted given that the angle between the benzyl ring plane and the N_2O_2 plane of 3.9°. This distortion could be due to the intermolecular metal–aromatic interactions present in the packing. No further π–π stacking or hydrogen bonds are observed.

UV-vis spectroscopy. Diffuse reflectance spectra powder samples of H_2L1, **1** and **2** were recorded in the UV-vis range. The normalized Kubelka–Munk functions plotted against the wavelength is shown in Fig. 4. The electronic spectra of H_2L1 show large bands between 200 and 400 nm that are attributed to π–π* transitions of the aromatic cycle and the conjugated systems. The electronic spectra of **1** and **2** are similar.

Table 3 Inclination of the planar complexes with the stacking direction; the stacking distance calculated as the distance between the metal and the planes calculated through the above and below complexes within the stack; twist angles as a measure of the rotation between the pairs of complexes as depicted in Fig. 2[a]

	Inclination (°)	Stacking distance (A)	Twist angles (°)
1·$CHCl_3$	75.71(3)	3.229 and 3.513	−92.0
1·H_2O	57.27(2)	3.312 and 3.440	−97.7
1·*x*solv	71.66(2)	3.299 and 3.334	−89.4
2·MeOH	70.52(3)	3.317 and 3.405	−91.7
3	79.40	3.275 and 3.353	180

[a] All planes were calculated through all non-hydrogen atoms of the complexes.

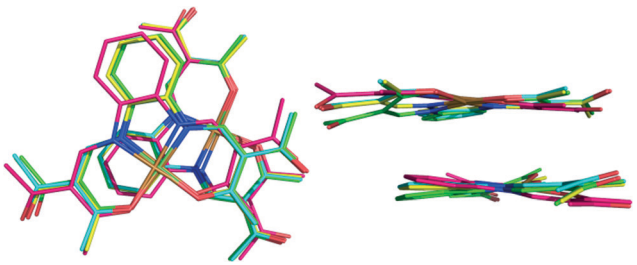

Fig. 2 Superposition of adjacent complexes from within a stack, superposed by pair fitting of the central metal atoms and the primary coordination sphere of both molecules (10 pairs). The top left view shows a similar orientation; the right side view shows the intermolecular distance. Carbon atoms are drawn in magenta for **1**·$2H_2O$, in cyan for **1**·*x*solv, in green for **1**·$CHCl_3$ and in yellow for **2**·MeOH.

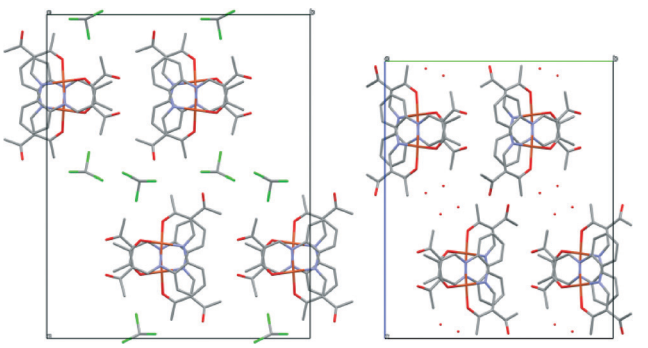

Fig. 3 Left: unit cell packing of **1**·$CHCl_3$; right: **1**·$2H_2O$ as seen along the stacking direction. The larger $CHCl_3$ molecules prevent a denser packing resulting in the expansion of the unit cell parameters (vertical). The intermolecular distance across the figure is controlled by the inclination of the complexes with respect to the stacking direction.

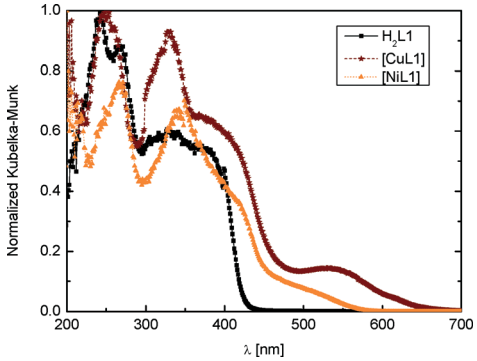

Fig. 4 Electronic spectra of H_2L1, **1** and **2**.

They both present a band at 252 nm for **1** and at 266 nm for **2** that can be attributed to π–π* transitions of the aromatic cycle and the conjugated systems of the ligand. Another intense band appears at 328 nm for **1** and at 341 nm for **2**, which is most likely a charge transfer band. A second band is observed at around 536 nm for **1** and at around 500 nm for **2** that can be attributed to the d–d-transitions of the metal. This band is less obvious in the case of **2** because it is a shoulder of the next band. The spectra of complexes **1** and **2** are in agreement with the colour of the complexes: brown for **1** and orange for **2**. The UV-vis spectra of **1** and **2** in different solvents ($CHCl_3$, DMSO, and pyridine) were recorded and are given in the ESI (S13–14†). **1** shows a strong solvatochromic shift from brown in $CHCl_3$ to green in pyridine. The shift in the colour of the solution is due to a shift of the d–d-transitions of the metal (550 nm in $CHCl_3$ to 595 nm in pyridine) as the coordination strength of the solvent increases. Such solvatochromism is not observed for the Ni(II) complex **2**.

Magnetic measurements. The nickel complex **2** is diamagnetic.[12] Magnetic measurements were performed on the powder samples of copper complexes **1** and **3** as a function of temperature. In Fig. 5, the reciprocal susceptibility $1/\chi_M$ is plotted *vs.* temperature. Both sets of data were appropriately fitted with the Curie–Weiss equation, $\chi_M = C/(T - \Theta)$, where C is the Curie constant and Θ the Weiss constant. Both complexes exhibit weak antiferromagnetic coupling with

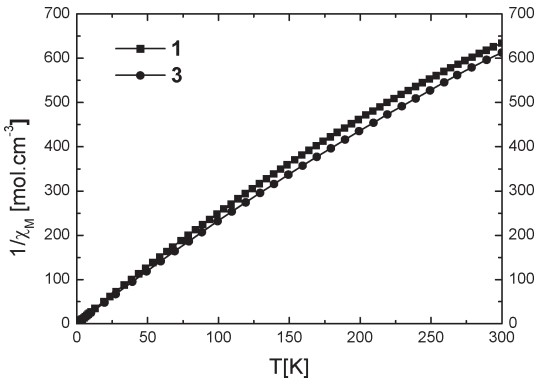

Fig. 5 Temperature dependence of the magnetic susceptibility measurements of the powder samples **1** and **3** between 300 K and 2 K. The $1/\chi_M$ *vs.* T plots are given.

C = 0.46(2) K and Θ = −9(1) K for **1** and C = 0.48(2) K and Θ = −7(1) K for **3**. The Curie constant is in the region expected for Cu(II) complexes with one unpaired electron.[17] The Curie plot is not strictly linear indicating some weak interactions in agreement with the Weiss constant magnitudes, which can be attributed to the different intermolecular interactions observed in the crystal packings.

Conclusions

The present structural report complements the previous article by Wolf and Jäger which described the synthesis of Schiff base complexes with Cu(II) and Ni(II).[12] Indeed, these authors proposed that a penta-coordinated Cu(II) complex can be obtained by a coordination bond between the metal centre and a ketone function from a neighbouring complex. No such bond was found in the four crystal structures of the copper complexes which we have determined. Their hypothesis was built on the fact that the $d_{x^2-y^2}$ orbital of copper in a square planar geometry is too high in energy and populating this orbital with one electron is not worth the stabilisation that the square planar geometry would bring to the complex. Indeed, in the crystal structure of **1**·$CHCl_3$, we observed a distorted square planar geometry. This distortion will lower the symmetry and thus decrease the energy of the $d_{x^2-y^2}$ orbital. In the crystal structures of **1**·$2H_2O$, **1**·xH_2O·yMeOH and **3**, the distortion of the square planar coordination sphere is significantly weaker. Here metal–aromatic interactions between the copper centre and the benzyl ring of a neighbouring complex were observed, which can also lower the symmetry of the complex and therefore reduce the energy of the $d_{x^2-y^2}$ orbital. This is in line with the structure of the Ni(II) complex, **2**·MeOH, where the coordination sphere is close to an ideal square planar one without significant interactions between the complex molecules. As the $d_{x^2-y^2}$ orbital for this complex with one less d-electron is empty, its strong destabilisation has no effect on the total energy. The different electronic character of the copper and the nickel complexes also explain their different tendencies to show solvatochromism.[12] In solution, the copper centre can interact with the solvent molecules. This leads to a distortion of the square planar geometry and will lower the energy of the $d_{x^2-y^2}$ orbital. The strength of this interaction depends on the donating ability of the solvent and influences the splitting of the 3d orbitals of the copper centre. For the nickel complex no such interactions are necessary and no solvatochromism is observed.

Experimental

Synthesis

All reagents were of reagent grade and used without further purification. All solvents were of analytical grade and used without further purification.

Syntheses of ligands H_2L1 and H_2L2 were performed as described.[12] X-ray quality single crystals of H_2L1·0.5dioxane were obtained as yellow needles from vapour–vapour

diffusion between a solution of the ligand in dioxane and water. UV-vis H_2L1 (PTFE): λ_{max} = 241, 268 and 328 nm (Fig. 4).

[CuL1] (**1**):[12] copper acetate monohydrate (0.39 g) and H_2L1 (0.66 g) were vigorously stirred in methanol (30 mL) overnight at room temperature,[9] resulting in a brown powder which was filtered, washed twice with ethanol (15 mL) and dried under vacuum. Yield: 0.6 g (75%). IR (KBr): $\bar{\nu}$ = 1652 (C═O, $COCH_3$), 1569 (C═O, $COCH_3$) cm^{-1}. CHN (%): exp. (theo.) for $C_{18}H_{18}CuN_2O_4$: C, 55.21 (55.45); H, 4.38 (4.65); N, 7.10 (7.18). UV-vis (PTFE): λ_{max} = 251, 328 and 536 nm.

Three solvates were obtained as single crystals suitable for X-ray crystallography: **1**·$CHCl_3$ crystals were obtained from trichloromethane as brown needles, **1**·$2H_2O$ crystals were obtained from THF as brown prisms and **1**·xH_2O·yMeOH from a MeOH–EtOH mixture.

[NiL1] (**2**):[12] nickel acetate tetrahydrate (0.50 g) and H_2L1 (0.66 g) were vigorously stirred in methanol (30 mL) overnight at room temperature.[9] The resulting orange powder was filtered, washed twice with ethanol (15 mL) and dried under vacuum. Yield: 0.6 g (75%). IR (KBr): $\bar{\nu}$ = 1653 (C═O, $COCH_3$), 1573 (C═O, $COCH_3$) cm^{-1}. CHN (%): exp. (theo.) for $C_{18}H_{18}NiN_2O_4$: C, 56.15 (55.98); H, 4.71 (4.59); N, 7.27(7.30). UV-vis (PTFE): λ_{max} = 266 and 340 nm.

Single crystals suitable for X-ray crystallography of **2**·MeOH were obtained from solvothermal synthesis with a saturated solution of **2** in methanol. The solution was heated to 80 °C for one day in a solvothermal bomb then left to cool overnight in a turned-off oven. Orange needles were collected.

[CuL2] (**3**):[12] copper acetate monohydrate (4.65 g) and H_2L2 (10 g) were dissolved in methanol (175 mL).[9] The solution was then refluxed for 2 min. After cooling, the brown precipitate was filtered and dried in vacuum. Single crystals suitable for X-ray crystallography were obtained from the mother liquor in the fridge as violet crystals. Yield: 9.28 g

Table 4 Crystallographic data for H_2L1·0.5dioxane, **1**·$CHCl_3$, **1**·$2H_2O$, **1**·*x*solv, **2**·MeOH and **3**

	H_2L1·0.5dioxane	**1**·$CHCl_3$	**1**·$2H_2O$
Formula	$C_{18}H_{20}N_2O_4$, 0.5($C_4H_8O_2$)	$C_{18}H_{18}N_2O_4Cu$, $CHCl_3$	$C_{18}H_{18}N_2O_4Cu$, 2(H_2O)
FW (g mol^{-1})	372.41	509.25	425.93
System	Monoclinic	Orthorhombic	Orthorhombic
Space group	*C*2/*c*	*Aba*2	*Pbca*
λ (Å)	0.71073	0.71073	0.71073
a (Å)	7.4692(8)	27.317(3)	8.025(1)
b (Å)	22.575(2)	22.2583(14)	19.28(1)
c (Å)	22.4145(14)	6.9575(5)	23.39(1)
	β (°) = 91.242(6)		
Volume (Å^3)	3778.6(6)	4230.4(6)	3620.0(2)
Z	8	8	8
T (K)	150	150	150
F(000)	1584	2072	1768
2θ (°)	47.06	50.76	50.48
Refl. collected	9812	15 226	
Unique/>2sigma(*I*)	2692/2057	3875/3207	3421/3129
Parameters	248	266	260
R_1 (all)[a]	0.0691 (0.0899)	0.0596 (0.0766)	0.0346 (0.0383)
ωR_2 (all)[b]	0.1648 (0.1808)	0.1213 (0.1310)	0.0950 (0.0987)
GooF	1.075	1.026	1.028
	1·*x*solv	**2**·MeOH	**3**
Formula	$C_{18}H_{18}N_2O_4Cu$	$C_{18}H_{28}N_2O_4Ni$, (C H_4 O)	$C_{22}H_{26}N_2O_8Cu$
FW (g mol^{-1})	389.88	417.08	510.00
Crystal system	Monoclinic	Monoclinic	Monoclinic
Space group	$P2_1/c$	$P2_1/c$	$P2_1/c$
λ (Å)	0.71073	0.71073	0.71073
a (Å)	11.2596(2)	11.1128(5)	6.74840(10)
b (Å)	23.9363(4)	23.9480(10)	21.9827(3)
c (Å)	6.9871(2)	7.1300(3)	16.0526(2)
β (°)	103.591(2)	103.599(5)	105.1720(10)
Volume (Å^3)	1830.38(7)	1844.31(14)	2298.37(6)
Z	4	4	4
T (K)	150	150	200
F(000)	804	872	1060
2θ (°)	50.48	50.48	54.946
Refl. collected	16 627	11 832	19 693
Unique/>2sigma(I)	3403/3144	3349/2289	5269
Parameters	231	250	302
R_1 (all)[a]	0.0408 (0.0438)	0.0537 (0.0941)	0.0401 (0.0656)
ωR_2 (all)[b]	16 627 (0.1134)	0.1136 (0.1353)	0.0960 (0.1067)
GooF	1.060	1.037	1.038

[a] $R_1 = \sum||F_o| - |F_c||/\sum|F_o|$. [b] $\omega R_2 = [\sum[w(F_o^2 - F_c^2)^2]/\sum w(F_o^2)^2]^{1/2}$, $w = 1/[\sigma^2(F_o^2) + (aP)^2 + bP]$, where $P = [F_o^2 + 2(F_c^2)]/3$.

(82%). CHN (%): exp. (theo.) for $C_{20}H_{22}CuN_2O_6$: C, 51.81 (51.63); H, 5.14 (5.11); N, 5.49 (5.54). MS (DEI^+) [m/z(%)]: 509 (100) $[M]^+$, 464 (15), 345 (50), 273 (28).

Physical measurements

IR spectra were recorded using a Shimadzu FTIR-84005 spectrometer using KBr discs at room temperature. Electronic spectra in the solid state were recorded with a CARY 5E spectrophotometer using polytetrafluoroethylene (PTFE) as a reference. CHN analyses were performed at MEDAC Ltd (UK). Mass spectra were recorded with a Jeol MS-700 device. The ionisation method used was DEI^+. Magnetic measurements were performed with a Quantum Design MPMSXL-5 SQUID magnetometer. The measurements were carried out at 0.7 T for **1** and 0.05 T for **2** in sweep mode (10 K min^{-1}) between 300 K and 10 K and in settle mode (2 K min^{-1}) between 10 K and 2 K. The data were corrected for the magnetisation of the sample holder and the diamagnetism of the ligand using tabulated Pascal's constants.

Single crystal X-ray structure determination

Crystals were mounted on a nylon loop with paratone or grease and flash-cooled in a N_2 gas stream. The data were collected using MoKα (λ = 0.71073 Å) radiation using a MAR345 image plate except for **3** which was measured using a KappaCCD detector. The structures were solved by direct methods using SHELXS[13] and refined by full least-squares on $|F^2|$ using SHELXL97.[13] All of the non-hydrogen atoms were refined with anisotropic temperature factors. The hydrogen atoms were placed in calculated positions in a riding model with the isotropic temperature factors fixed at $1.2U_{eq}$ of the parent atoms (1.5 for methyl groups). The crystallographic and refinement data are summarised in Table 4.

Acknowledgements

This work was funded by the Fonds National de la Recherche Scientifique (FNRS) and the University of Bayreuth.

Notes and references

1 K. C. Gupta and A. K. Sutar, *Coord. Chem. Rev.*, 2008, **252**, 1420–1450.
2 (*a*) T. Fasina, O. Ogundele, F. Ejiah and C. Dueke-Eze, *Int. J. Biol. Chem.*, 2012, **6**, 24–30; (*b*) D.-D. Qin, Z.-Y. Yang and B.-D. Wang, *Spectrochim. Acta, Part A*, 2007, **68**, 912–917.
3 (*a*) B. Weber and E.-G. Jäger, *Eur. J. Inorg. Chem.*, 2009, **4**, 465–477; (*b*) T. M. Pfaffeneder, S. Thallmair, W. Bauer and B. Weber, *New J. Chem.*, 2011, **35**, 691–700; (*c*) S. Schlamp, B. Weber, A. D. Naik and Y. Garcia, *Chem. Commun.*, 2011, **47**, 7152–7154.
4 O. Bienemann, A.-K. Froin, I. dos Santos Vieira, R. Wortmann, A. Hoffmann and S. Herres-Pawlis, *Z. Anorg. Allg. Chem.*, 2012, **638**, 1683–1690.
5 R. N. Patel, V. L. N. Gundla and D. K. Patel, *Polyhedron*, 2008, **27**, 1054–1060.
6 X. Dong, Y. Li, Z. Li, Y. Cui and H. Zhu, *J. Inorg. Biochem.*, 2012, **108**, 22–29.
7 M. Orio, O. Jarjayes, H. Kanso, C. Philouze, F. Neese and F. Thomas, *Angew. Chem., Int. Ed.*, 2010, **49**, 4989–4992.
8 (*a*) T. N. Mandal, S. Roy, A. K. Barik, S. Gupta, R. J. Butcher and S. K. Kar, *Polyhedron*, 2008, **27**, 3267–3274; (*b*) A. Biswas, M. G. B. Drew and A. Ghosh, *Polyhedron*, 2010, **29**, 1029–1034; (*c*) K. Sundaravel, E. Suresh and M. Palaniandavar, *Inorg. Chim. Acta*, 2009, **362**, 199–207.
9 W.-K. Dong, X.-N. He, H.-B. Yan, Z.-W. Lv, X. Chen, C.-Y. Zhao and X.-L. Tang, *Polyhedron*, 2009, **28**, 1419–1428.
10 P. K. Bhaumik, S. Jana and S. Chattopadhyay, *Inorg. Chim. Acta*, 2012, **390**, 167–177.
11 M. M. Bhadbhade and D. Srinivas, *Inorg. Chem.*, 1993, **32**, 5458–5466.
12 L. Wolf and E.-G. Jäger, *Z. Anorg. Allg. Chem.*, 1966, **346**, 76–91.
13 G. Sheldrick, *Acta Crystallogr., Sect. A: Found. Crystallogr.*, 2008, **64**, 112–122.
14 (*a*) C. K. Johnson and M. N. Burnett, *ORTEP-III*, Oak-Ridge National Laboratory, Oak-Ridge, TN, 1996; (*b*) L. Farrugia, *J. Appl. Crystallogr.*, 1997, **30**, 565.
15 (*a*) F. Robert, P. L. Jacquemin, B. Tinant and Y. Garcia, *CrystEngComm*, 2012, **14**, 4396–4406; (*b*) D. A. Safin, K. Robeyns and Y. Garcia, *RSC Adv.*, 2012, **2**, 11379–11388; (*c*) D. A. Safin and Y. Garcia, *RSC Adv.*, 2013, **3**, 6466–6471.
16 W. Bauer, T. Ossiander and B. Weber, *Z. Naturforsch., B: J. Chem. Sci.*, 2010, **65b**, 323–328.
17 M. Friedrich, J. C. Gálvez-Ruiz, T. M. Klapötke, P. Mayer, B. Weber and J. J. Weigand, *Inorg. Chem.*, 2005, **44**, 8044–8052.

